PHYSICAL REVIEW B VOLUME 25, NUMBER 6 15 MARCH 1982

Self-consistent extended-muffin-tin orbital energy-band method: Application to LiC_6

R. V. Kasowski
Central Research and Development Department, E. I. du Pont de Nemours and Company, Experimental Station, Wilmington, Delaware 19898
(Received 13 April 1981; revised manuscript received 17 August 1981)

The extended-muffin-tin orbital (EMTO) energy-band method has been made self-consistent by fast-Fourier-transforming the non-muffin-tin charge density. The EMTO method is used here to calculate self-consistent energy bands for Li-intercalated graphite. The Li s and p states are found to be empty. The carbon π states near the Fermi energy are found to be strongly distorted from that of pure graphite.

I. INTRODUCTION

The extended-muffin-tin-orbital- (EMTO) energy-band method[1] has been applied non-self-consistently to a variety of problems: (a) CO molecules interacting at a Ni(001) surface,[1] (b) polymers with and without dopants,[2] and (c) Si-SiO_2 interface.[3] The purpose of this paper is to present a self-consistent version, which can be applied generally. This new scheme will be demonstrated with Li-intercalated graphite.

The EMTO method is applicable to a wide variety of problems because the complete potential is treated. It is convenient to use even for very complex geometries, because the potential is easily divided into spherically symmetric muffin-tin potentials and a non-muffin-tin part. The non-muffin-tin part includes the nonspherical contributions to the potential throughout the unit cell, including inside the muffin-tin spheres. The non-muffin-tin potential is smooth everywhere, thus allowing use of a fast Fourier[4] transform for representation in plane waves. Self-consistency is facilitated by dividing the charge density into a spherically symmetric muffin-tin part and a non-muffin-tin part that is smooth enough to be fast-Fourier-transformed. The Coulomb potential is easily obtained for the self-consistent iterations. The simple forms for the charge density and potential enable one to easily write an expression for total energy.

Graphite and graphite-intercalation compounds continue to be widely investigated.[5] In graphite intercalated with alkali-metal atoms, it is thought that the s electrons are donated to the conduction band. Holzwarth *et al.*[6] support this interpretation with a non-self-consistent-field (SCF) energy-band calculation for LiC_6. They find the bands to be in quantitative agreement with the corresponding bands of undoped graphite. They also found the Li $2s$ band to be ~ 1.7 eV above E_F. More recently, Holzwarth[7] performed a self-consistent pseudopotential[8] calculation for LiC_6. The Li $2s$ band was found to be ~ 1.0 eV above E_F. Overall, the pseudopotential results resemble the earlier non-SCF calculations.

Our calculations on LiC_6 were carried out with two different types of muffin-tin orbitals. The first type is that used in the original formulation of the muffin-tin-orbital energy-band method.[9] These MTO's are constructed from the radial solutions of the muffin-tin potential and the spherical Bessel function orthogonalized to the core states as in the orthogonalized-plane-wave (OPW) method. Andersen[10] has since advocated a second type of linearized muffin-tin orbital whereby the energy derivative of the radial solution of the muffin-tin potential replaces the Bessel function part of the muffin-tin orbital. We will show that similar results are obtained with either type of muffin-tin orbitals. Finally, we will show that the techniques of the EMTO method can be used to extend the augmented spherical wave[11] (ASW) method to non-muffin-tin potentials.

The SCF-EMTO method is presented in Sec. II. Our results for LiC_6 are shown in Sec. III. Section IV contains the conclusions. The Appendix gives a detailed derivation of the method with test results for Si and GaAs.

II. EXTENDED EMTO METHOD

The first step in using the EMTO method is to construct a potential, which is divided into a muffin-tin part $V_{\rm MT}(r)$ and a non-muffin-tin part $\Delta V(\vec{r})$. $V_{\rm MT}(r)$ is spherically symmetric and defined inside muffin-tin spheres centered at various atoms, with radius S. $\Delta V(\vec{r})$ is defined throughout the unit cell including the muffin-tin regions. $\Delta V(\vec{r})$ is made continuous everywhere by adding the value of the muffin-tin potential at the muffin-tin radius, $V_{\rm MTZ}$ inside the muffin tins. $V_{\rm MTZ}$ must then be subtracted from $V_{\rm MT}(r)$.

The EMTO method requires the definition of two types of muffin-tin orbitals. The first type $\chi_{lm}(E_1,\kappa^2,\vec{r},\vec{\tau})$ is constructed from the radial solution $\phi_{lm}(E_1,\vec{r},\tau)$ of the potential $V_{\rm MT}(r)$ at fixed energy E_1 for each atom $\vec{\tau}$ in the unit cell:

$$\chi_{lm}(E_1,\kappa^2,\vec{r},\vec{\tau})=\begin{cases} N_1[\phi_{lm}(E_1,r,\tau)+\omega_1\dot{\phi}_{lm}], & r\le S \\ -K_{lm}(\kappa,\vec{r},\tau), & r\ge S \end{cases} \tag{1}$$

where $\dot{\phi}$ is the derivative of ϕ with respect to energy and is orthogonal to ϕ. A complete discussion of linearized MTO's has been given by Andersen.[10] K_{lm} is the spherical Neumann function. N_1 and ω_1 are chosen to give a continuous wave function and first derivative. The spherical harmonics are also contained in the definitions of ϕ, $\dot{\phi}$, and K. The MTO's could have been defined with a Bessel function orthogonalized to the core states replacing $\dot{\phi}$ as was done in earlier work.[9] We will show that similar results are obtained with either type of MTO.

The second type of muffin-tin orbital, $p_{lm}^{\vec{k}}(\kappa,r,\tau)$, is constructed from the spherical Bessel and Neuman functions, J_1 and K_1, respectively,

$$p_{lm}=\begin{cases} N_1\left[J_1(\kappa r)+\omega_1\dfrac{dJ_{lm}(\kappa r)}{d\kappa^2}\right], & r\le S \\ -K_{lm}(\kappa r), & r\ge S\ . \end{cases} \tag{2}$$

N_1 and ω_1 are chosen to ensure continuity of the MTO tail K_{lm} and its first derivative at S. The important properties of p_{lm} are that it is (a) equal to the MTO χ_{lm} outside the muffin-tin radius, (b) smooth inside the muffin-tin spheres whereas χ_{lm} may have nodes, and (c) independent of the potential and need be evaluated only once.

A basis function $\Psi^{\vec{k}}(\vec{r})$ is now formed from a linear combination of MTO Bloch functions $\chi_{lm}^{\vec{k}}$:

$$\Psi^{\vec{k}}(\vec{r})=\sum_{\kappa^2}\sum_{\tau lm}C_{\tau lm}\chi_{lm}^{\vec{k}}(E_1,\kappa^2,\vec{r},\vec{\tau})\ . \tag{3}$$

A sum over κ^2 is included since for open structures[12] such as Si, it is necessary to use both short range MTO's ($\kappa^2<0$) and long range MTO's ($\kappa^2>0$) in the basis function. For close-packed metals, only one κ^2 is necessary.

The complete derivation of an arbitrary matrix element is given in the Appendix:

$$\langle\chi_1^{\vec{k}}\,|\,H-E\,|\,\chi_2^{\vec{k}}\rangle=\langle p_1^{\vec{k}}\,|\,\kappa_2^2+\Delta V+V_{\rm MTZ}\Theta-E\,|\,p_2^{\vec{k}}\rangle_{\rm unit\ cell}+\langle\chi_1^{\vec{k}}\,|\,-\nabla^2+V_{\rm MT}-E\,|\,\chi_2^{\vec{k}}\rangle_{\rm MT}$$
$$-\langle p_1^{\vec{k}}\,|\,\kappa_2^2+V_{\rm MTZ}\Theta-E\,|\,p_2^{\vec{k}}\rangle_{\rm MT}\ . \tag{4}$$

(This equation corrects misprints in earlier paper.[1]) 1 and 2 represent two sets of parameters κ^2, l, m, E, and τ necessary to define the MTO, $\chi_{lm}^{\vec{k}}\cdot p_j^{\vec{k}}$ ($j=1,2$) denotes the Bloch function formed from the smooth type of MTO. As indicated in the Appendix, integrations over the muffin-tin regions (MT) are easily performed because of spherical symmetry. The term involving integration over the unit cell is evaluated numerically and requires a full discussion. First, the unit cell is divided into polyhedra by dividing the three unit-cell vectors into sections roughly 0.35 Å long. Next the Bloch function $p_j^{\vec{k}}$ is evaluated at the same point in each polyhedron. The function $p_j^{\vec{k}}$ is sufficiently smooth that a fast Fourier transform (FFT) yields a finite-series representation:

$$p_j^{\vec{k}}(\vec{r}-\vec{\tau},S,\kappa^2)=\sum_{\vec{G}}M_{\vec{G}}\,e^{-i(\vec{G}-\vec{k})\cdot(\vec{r}-\vec{\tau})}\ . \tag{5}$$

The numerical integration over the unit cell in Eq. (4) is then performed by choosing an appropriate number of random points in a given polyhedron. The wave function $p_j^{\vec{k}}$, is evaluated at these random points and in all other polyhedra by using the inverse FFT of Eq. (5). Furthermore, the inverse FFT yields the wave function $p_j^{\vec{k}}$ for all atoms

with the same muffin-tin radius. The function $p_j^{\vec{k}}$ does not depend on the potential and is evaluated only once and then reused during iteration to self-consistency.

Poissons's equation can be solved by putting the charge density into a spherically symmetric part and a Fourier series. The charge density can be put in such convenient forms for self-consistent iteration by adding and subtracting the term $|\sum C_j^n p_j^{\vec{k}}|^2$:

$$\rho(r)=\sum_n \left[\left| \sum_j C_j^n \chi_j^{\vec{k}} \right|^2 - \left| \sum_j C_j^n p_j^{\vec{k}} \right|^2 \right]_{\mathrm{MT}} + \sum_n \left| \sum_j C_j^n p_j^{\vec{k}} \right|^2 , \tag{6}$$

where j represents τ, l, m, and k^2. The sum over occupied states is represented by n. C_j^n are the coefficients of the wave function. The first two terms provide a spherically symmetric charge density that goes to zero at the muffin-tin radius, S. The last term is smooth everywhere in the unit cell and is calculated on the same mesh of points as previously used to evaluate the MTO $p_j^{\vec{k}}$. Application of the FFT to this term yields a finite Fourier series which when added to the muffin-tin part gives the total charge density.

$$\rho(\vec{r})=\rho_{\mathrm{MT}}(|r|)+\sum \rho_{\vec{G}} e^{-i\vec{G}\cdot\vec{r}} . \tag{7}$$

It is now straightforward to solve Poissons's equation and obtain a radial Coulomb potential due to $\rho_{\mathrm{MT}}(r)$, a Madelung term due to the constant background $\rho_{G=0}$, and a plane-wave term due to

$$\sum_{G\neq 0} \rho_{\vec{G}} \exp(-i\vec{G}\cdot\vec{r}) .$$

The exchange potential is straightforward enough to evaluate, even though it depends nonlinearly on the charge density. The exchange potential is divided into a spherically symmetric part that depends only on the true muffin-tin charge density.

$$V_{\mathrm{sph}}^{\mathrm{ex}}(r)=f^{\mathrm{ex}}(\rho_{\mathrm{sph}}(r)) , \tag{8}$$

where

$$\rho_{\mathrm{sph}}(r)=\sum_n \left| \sum C_j^n \chi_j^{\vec{k}} \right|^2_{\mathrm{sph\ av}} ,$$

where n is a sum over occupied states, and f^{ex} is the exchange-potential function. To evaluate the nonspherical part of the exchange potential, Eq. 7 is used to evaluate the total charge density at all grid points in the unit cell.

$$\Delta V^{\mathrm{ex}}(\vec{r})=f_{\mathrm{ex}}(\rho(\vec{r}))-f_{\mathrm{ex}}(\rho_{\mathrm{sph}}(r)) . \tag{9}$$

The above expressions for charge density and Coulomb potential are in a convenient form to derive an equation for total energy per unit cell:

$$E_t=\sum \epsilon_i - \tfrac{1}{2}\int \rho(\vec{r})d\vec{r}\int \frac{2\rho(\vec{r}\,')}{|\vec{r}-\vec{r}\,'|}d\vec{r}\,' - \tfrac{1}{4}\int \alpha V_{\mathrm{ex}}\rho(\vec{r})d\vec{r}+\tfrac{1}{2}\sum{}' \frac{2Z^2}{R} , \tag{10}$$

where $\alpha V_{\mathrm{ex}}=-3\alpha(3\rho/\pi)^{1/3}$, and ϵ_i are the band-structure eigenvalues. These calculations are in progress. The above derivation follows precisely that of Ross and Johnson[13] and is not repeated here.

The above formalism is easily applied to molecules and thin films in conjunction with a superlattice.[8] In this model, molecules or films are separated sufficiently from neighboring molecules or films so that they do not interact. The main advantage of the superlattice model is that three-dimensional FFT's can be used to calculate the wave function and solve the nonspherical Coulomb potential.

The EMTO equations in Eq. (4) can be related to those of the LMTO method[10] by allowing the muffin tins to overlap and setting $\Delta V=0$. The LMTO formalism[10] is worked out only for $\kappa^2=0$. However, by using the EMTO formalism and FFT's, one can generalize the LMTO equations to any value of κ^2 or even to two sets of MTO's per atoms. Furthermore, for $\Delta V=0$, the integral over the unit cell in Eq. (4) becomes a simple sum over the reciprocal-lattice vectors $\vec{G}$.

Our method for treating nonspherical potentials and charge distributions could also be used to extend the augmented-spherical-wave (ASW) method of Williams *et al.*,[11] so that a general potential could be treated. Currently, the ASW method approximates the true potential by overlapping muffin tins as in the LMTO method. The wave function in the ASW method is defined as a linear combination of augmented spherical waves. The augmented spherical waves are defined in an equivalent manner to our MTO's in the interstitial region as both have identical tails. Inside the muffin tins, Williams *et al.* choose radial solutions at a specific energy to obtain continuous wave functions over the muffin-tin spheres whereas we have chosen the radial function and its first derivative

with respect to energy.

The first step in deriving their method for non-muffin-tin potentials is to apply the variational principle and obtain an equation similar to Eq. (A1) in the Appendix.

$$\langle h_l^{\vec{k}} | H-E | h_2^{\vec{k}} \rangle = \langle h_l^{\vec{k}} | -\nabla^2+V_{\mathrm{MT}}-E | h_2^{\vec{k}} \rangle_{\mathrm{MT's}} + \langle h_l^{\vec{k}} | \Delta V | h_2^{\vec{k}} \rangle_{\mathrm{MT's}} + \langle h_l^{\vec{k}} | -\nabla^2+\Delta V-E | h_2^{\vec{k}} \rangle_{\mathrm{interstitial}} . \quad (11)$$

h_j denotes the augmented spherical wave, and j denotes l, m, τ, and κ^2. One adds and subtracts the term in Eq. (A2). The rest of the derivation proceeds exactly as for the EMTO method. The Coulomb potential for the SCF procedure is also solved similarly.

III. BAND STRUCTURE OF LiC_6

A. Crystal structure and basis set

The crystal structure of LiC_6 consists of two-dimensional hexagonal carbon planes separated by Li intercalates.[14] The carbon planes are dilated by about 1% over that of pure carbon (hexagonal lattice constant $a=4.85$ Å). The carbon layers are stacked in direct registry with respect to each other so that there is only 1 unit of LiC_6 in the primitive cell. The distance between carbon layers ($c=3.706$ Å) is 10% over that in pure graphite. Finally, the Li atoms are arranged midway between the C layers so that there are six C atom nearest neighbors below and above each Li.

As discussed in the previous section, MTO's are defined by the energy at which the radial solution of the muffin tin potential is calculated and also by the energy κ^2 of the Neuman function tail. The energy parameter was taken to be -4.0 eV, which is near E_F. The κ^2 parameter was chosen to be -0.4, -0.1, 0.3, and 0.5 Ry. $\kappa^2=0.3$ Ry gave the lowest eigenvalues. Only the s and p^3 MTO's were included in the basis set. Thus, at a general $\vec{k}$ point, the matrix size is 28×28.

The crystal potential was obtained using the Hedin-Lundquist[15] χ_α exchange approximation. The charge density was calculated using a 3-k point-sampling scheme based on the special points for a hexagonal film.[16]

B. Band structure of LiC_6

The energy bands for LiC_6 using the Hedin-Lundquist exchange are shown in Fig. 1. The bands have been labeled according to the convention of Holzwarth *et al.*[6] The carbon π and σ bands are represented by dashed and full lines, respectively. Bands derived primarily from the Li s and p states have been darkened to distinguish them from C states. It is clear from Fig. 1 that the Li s and p states are empty.

In Fig. 2, the non-self-consistent energy bands are presented. The starting potential here was constructed by overlapping neutral atom charge densities. Comparison of Figs. 1 and 2 shows that the major effect of iterating the non-SCF bands in Fig. 2 is to change the position of the Li states relative to the C states. At the Γ point, the Li s state is 4 eV above the π states for the non-SCF. For the SCF results in Fig. 1, the Li s state is only 2.0 eV above the π states. The dispersion of the bands in $\vec{k}$ space and the positions of the C π and σ bands are quite similar for the SCF and non-SCF results.

Eberhardt *et al.*[17] have identified several features of LiC_6 at the Γ point, using angle-resolved photoemission. In Table I, a comparison is made of these experimentally identified features and our SCF results. Because of the limited number of $\vec{k}$ points used in sampling the Brillouin zone, the determination of E_F is approximate. The MTO band structure compares well with experiment for all levels.

Eberhardt *et al.*[17] also performed Li core-threshold photoyield spectra. Two peaks were

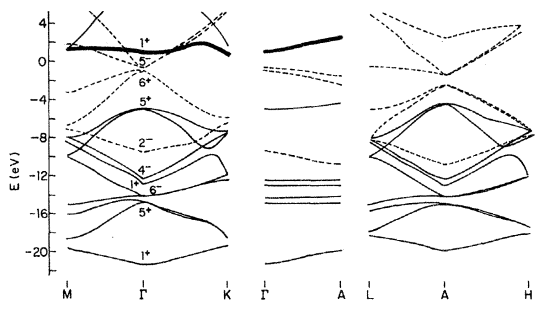

FIG. 1. SCF energy bands of LiC_6 using parameters $\kappa^2=-0.1$ Ry and $E=-0.3$ Ry.

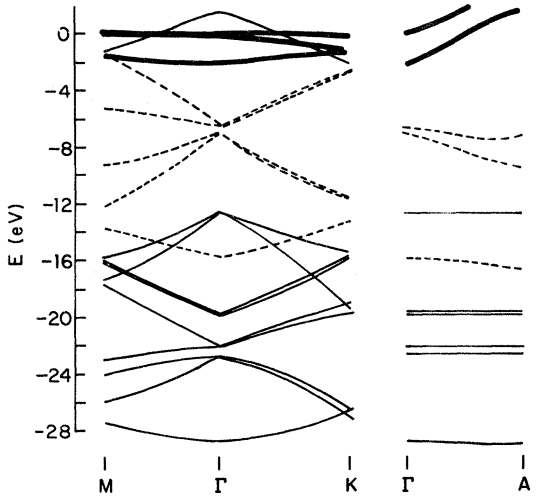

FIG. 2. Non-SCF energy bands of LiC_6.

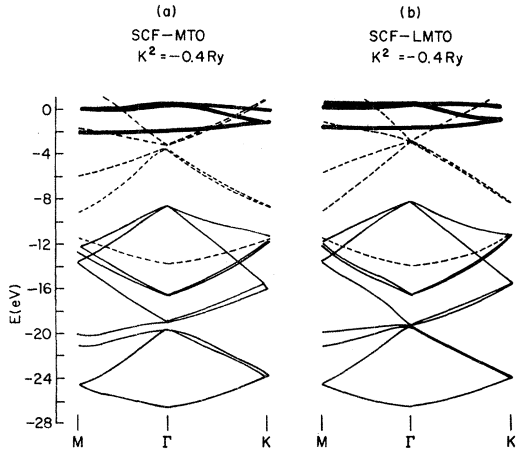

FIG. 3. Comparison of energy bands of LiC_6 using orthogonalized MTO's and linearized MTO's both with parameters $E=-0.3$ Ry and $\kappa^2=-0.4$ Ry.

found at approximately 1.4 and 6 eV above E_F. Inspection of Fig. 1 indicates a peak due to Li states at 1.5 eV above E_F.

The Li p states hybridize very strongly with the C states above E_F. Their energies depend strongly on which κ^2 is used in the basis set. We have not displayed these unfilled states as we are not sure of their positions.

Finally, we wish to compare the difference in results obtained with MTO's formed with an orthogonalized Bessel function as with an LMTO. In Fig. 3, SCF bands using orthogonalized MTO's are shown along with SCF bands using SCF-linearized MTO's. The MTO parameters E and κ^2 were -0.3 and -0.4 Ry, respectively, for both basis sets. The two sets of bands are too similar to say which compares better with experiment.

TABLE I. Γ-point binding energies relative to E_F (in eV).

Symmetry label	EMTO	Expt.
1^+	-21.3	-22.5 ± 0.4
$6^-,5^+$	-14.79	-15.2 ± 0.5
	-14.2	
$4^-,1^+$	-12.9	-13 ± 0.5
	-12.39	
2^-	-9.49	-9.3 ± 0.3
5^+	-5.0	-5.0 ± 0.4
$5^-,6^+$	-0.991	-0.5 ± 0.03
	-0.716	
	0.902	$+1.45$ eV

We can see the effect of different choices of the parameter κ^2 by comparing Fig. 1 ($\kappa^2=0.3$ Ry) with Fig. 3 ($\kappa^2=-0.4$ Ry). The positions of the π states are about 0.4 eV closer to the Li states for the $\kappa^2=0.3$ Ry. This value is more in line with experiment as discussed earlier.

IV. CONCLUSIONS

Self-consistent energy bands have been obtained for LiC_6 which agree well with photoemission data. In the future, our SCF computer programs will be extended so that a double set of MTO's on each atom can be used as a trial basis function. A double set of MTO's will improve the agreement between theory and experiment over a wider energy range and allow us to calculate unfilled states more accurately. Currently the programs are being developed to calculate total energies.

ACKNOWLEDGMENTS

I would like to thank Dr. A. R. Williams for providing a subroutine to implement the Hedin-Lundquist exchange. I would like to thank Dr. E. Caruthers for helpful discussions and implementation of the Hedin-Lundquist exchange. Dr. D. Scofield and Dr. A. Suna are acknowledged for helpful discussions about FFT's. I am grateful to Dr. N. Holzwarth for communicating her LiC_6 results prior to publication. I wish also to thank Dr.

S. Floodmark for furnishing a program with which to calculate symmetry. I wish to thank Dr. F. Herman for helpful discussions on all phases of this work and also helping to implement the symmetry program of Dr. Floodmark. Dr. Herman also made a detailed comparison of results obtained with previous linear combination of muffin-tin orbital programs and the new EMTO programs. Finally, I thank Dr. W. Hsu for a critical reading of this manuscript.

APPENDIX

The matrix elements of the Hamiltonian can be divided into integrations over the muffin-tin (MT) and interstitial regions:

$$\langle \chi_1^{\vec{k}} | -\nabla^2+V_{\rm MT}+\Delta V-E | \chi_2^{\vec{k}} \rangle = \langle \chi_1^{\vec{k}} | -\nabla^2+V_{\rm MT}-E | \chi_2^{\vec{k}} \rangle_{\rm MT's} + \langle \chi_1^{\vec{k}} | \Delta V | \chi_2^{\vec{k}} \rangle_{\rm MT's} + \langle \chi_1^{\vec{k}} | -\nabla^2+\Delta V-E | \chi_2^{\vec{k}} \rangle_{\rm interstitial} . \quad \text{(A1)}$$

The notations 1 and 2 represent two arbitrary sets of MTO parameters l, m, κ^2, E, and τ. The major obstacle to solving the equation is that the interstitial integration is discontinuous. Thus, the muffin-tin term will be added and subtracted,

$$\langle p_1^{\vec{k}} | -\nabla^2+\Delta V+V_{\rm MTZ}-E | p_2^{\vec{k}} \rangle_{\rm MT} , \quad \text{(A2)}$$

so that the discontinuity is eliminated and the term $\langle \chi_1^{\vec{k}} | \Delta V | \chi_2^{\vec{k}} \rangle_{\rm MT}$ is approximately cancelled. $V_{\rm MTZ}$ is the value of $V_{\rm MT}(r)$ at the muffin-tin radius.

The MTO $p_j^{\vec{k}}$ has been previously defined in Sec. II. We will only add that $p_j^{\vec{k}}=\chi_j^{\vec{k}}$ at the muffin-tin radius and that this function is smooth throughout the unit cell. The MTO $\chi_j^{\vec{k}}$ behaves differently in that it contains rapid oscillations introduced by solutions to the Schrödinger equation from which it is constructed.

Equation (A1) now becomes

$$\begin{aligned}\langle \chi_1^{\vec{k}} | -\nabla^2+V_{\rm MT}+\Delta V-E | \chi_2^{\vec{k}} \rangle = {} & \langle \chi_1^{\vec{k}} | -\nabla^2+\Delta V-E | \chi_2^{\vec{k}} \rangle_{\rm intersphere} \\ & + \langle p_1^{\vec{k}} | -\nabla^2+\Delta V+V_{\rm MTZ}-E | p_2^{\vec{k}} \rangle_{\rm MT} \\ & + \langle \chi_1^{\vec{k}} | -\nabla^2+V_{\rm MT}-E | \chi_2^{\vec{k}} \rangle_{\rm MT} - \langle p_1^{\vec{k}} | -\nabla^2+V_{\rm MTZ}-E | p_2^{\vec{k}} \rangle_{\rm MT} \\ & + \langle \chi_1^{\vec{k}} | \Delta V | \chi_2^{\vec{k}} \rangle_{\rm MT} - \langle p_1^{\vec{k}} | \Delta V | p_2^{\vec{k}} \rangle_{\rm MT} . \end{aligned} \quad \text{(A3)}$$

The first two terms are combined and the last two terms are approximately equal and cancel. Further, $-\nabla^2 p_j^{\vec{k}}=\kappa^2 p_j^{\vec{k}}$ so that

$$\langle \chi_1^{\vec{k}} | -\nabla^2+V_{\rm MT}+\Delta V-E | \chi_2^{\vec{k}} \rangle = \langle p_1^{\vec{k}} | \kappa_2^2+\Delta V+V_{\rm MTZ}\Theta-E | p_j^{\vec{k}} \rangle_{\rm unit\ cell} + \langle \chi_1^{\vec{k}} | -\nabla^2+V_{\rm MT}-E | \chi_2^{\vec{k}} \rangle - \langle p_1^{\vec{k}} | \kappa_2^2+V_{\rm MTZ}\Theta-E | p_2^{\vec{k}} \rangle_{\rm MT} . \quad \text{(A4)}$$

The function Θ is equal to unity inside the muffin-tin spheres and zero outside. $V_{\rm MTZ}\Theta$ must be added to ΔV which otherwise would be discontinuous at the muffin-tin boundaries.

The integrals over the muffin-tin spheres have been discussed in detail in previous work[9] and will only be summarized here. One can reduce the multicentered Bloch functions $\chi_j^{\vec{k}}$ and $p_j^{\vec{k}}$ to single-center sums within a given sphere. For example, the MTO at site τ_1 can be expanded about τ_i:

$$\chi_1^{\vec{k}}(\vec{r}-\vec{\tau}_1)=N_1[\phi_i(\vec{r}-\vec{\tau}_i)+\omega_i\dot{\phi}(\vec{r}-\vec{\tau}_i]\delta_{i1} + \sum_{\rm LM} J_{\rm LM}(r-\tau_i)\Lambda_{{\rm LM},1} , \quad \text{(A5)}$$

where N_1 and ω_i are normalization constants. $J_{\rm LM}$ is a Bessel function for r greater than the muffin-tin radius S, and is a combination of ϕ_i and $\dot{\phi}_i$ appropriately normalized for $r<S$. Thus, Eq. (A5) enables the integrals over the MT volumes to be reduced to radial integrals.

The remaining integral is performed numerically by dividing the unit cell into polyhedra and choosing random points within a polyhedron. The wave function $p_j^{\vec{k}}$ is evaluated at an identical point within each of the polyhedra. Application of the fast Fourier transform gives a finite plane-wave expression:

$$p_j^{\vec{k}} = \sum M_{\vec{G}} e^{-i(\vec{G}-\vec{k})\cdot(\vec{r}-\vec{r}_i)} .$$

The inverse FFT is used to generate all the required values of the wave function at the random points.

The key approximation in the EMTO method is that

$$\langle \chi_1^{\vec{k}} | \Delta V | \chi_2^{\vec{k}} \rangle_{\mathrm{MT}} \sim \langle p_1^{\vec{k}} | \Delta V | p_2^{\vec{k}} \rangle .$$

This approximation is valid near the muffin-tin radius even though ΔV has its largest value because $\chi_1^{\vec{k}}$ is equal to $p_1^{\vec{k}}$. In the inner portion of the muffin-tin sphere, $\chi_1^{\vec{k}}$ deviates from $p_2^{\vec{k}}$, but ΔV becomes very small.

In order to test the above approximation, energy-band calculations were performed for Si with the EMTO method and the LCMTO (Ref. 9) method for identical potentials. In the LCMTO method, the potential is expanded in spherical harmonics within atomic Wigner-Seity cells about each atom. Thus, there are no approximations to the potential. The two-band calculations agree to within 0.01 eV,[18] thus supporting our conclusion that the approximation used in the EMTO method is valid.

Finally, a self-consistent energy-band calculation for Si is in close agreement with the linearized augmented-plane-wave (LAPW) results of Hamann.[19] At the major symmetry points we obtain in eV (Hamann's results are in parenthesis): γ_1 −11.87 (−12.02), γ'_{25} 0.0 (0.0), γ_{12} 2.44 (2.49), γ'_2 3.38 (3.18), X_1 −7.88 (−7.84), X_4 −2.92 (−2.82), X_1 0.57 (0.55), X_4 10.18 (10.32), L'_2 −9.69 (−9.64), L_1 −6.98 (−7.06), L'_3 −1.27 (−1.16), L_1 1.47 (1.40), and L_3 3.25 (3.37). For GaAs we obtain in eV: γ_1 −11.87, γ_{15} 0.0, γ_1 1.23, γ_{15} 3.98, X_1 −9.93, X_3 −6.45, X_5 −2.63, X_1 1.54, L_1 −10.59, L_1 −6.38, L_3 −1.15, L_1 1.43, and L_3 4.84. The above results suggest the high level of accuracy obtainable with the EMTO method.

[1] R. V. Kasowski and E. Caruthers, Phys. Rev. B 21, 3200 (1980).

[2] R. V. Kasowski, E. Caruthers, and W. Y. Hsu, Phys. Rev. Lett. 44, 676 (1980); R. V. Kasowski, W. Y. Hsu, and E. B. Caruthers, J. Chem. Phys. 79, 4896 (1980).

[3] F. Herman, I. P. Batra, and R. V. Kasowski, *The Physical Chemistry of SiO_2 and Its Interfaces* (Pergamon, New York, 1978), p. 339.

[4] C. O. Brigham, *The Fast Fourier Transform* (Prentice-Hall, Englewood Cliffs, N.J., 1974).

[5] J. E. Fischer and T. E. Thompson, Phys. Today 31, 36 (1978).

[6] N. A. W. Holzwarth, S. Rabii, and T. A. Girifalco, Phys. Rev. B 18, 5190 (1978).

[7] N. A. W. Holzwarth (private communication).

[8] S. G. Louie, K. M. Ho, J. K. Chelikowsky, and M. L. Cohen, Phys. Rev. B 15, 4527 (1977).

[9] O. K. Andersen and R. V. Kasowski, Phys. Rev. B 4, 1064 (1971); R. V. Kasowski and O. K. Andersen, Solid State Commun. 11, 799 (1972).

[10] O. K. Andersen, Phys. Rev. B 12, 3060 (1975).

[11] A. R. Williams, J. Kübler, and C. D. Gelatt, Jr., Phys. Rev. B 19, 6094 (1979).

[12] R. V. Kasowski, Phys. Rev. B 14, 3398 (1976).

[13] M. Ross and K. W. Johnson, Phys. Rev. 2, 4709 (1970).

[14] D. Guerard and A. Herold, Carbon 13, 337 (1975).

[15] L. Hedin and B. I. Lundquist, J. Phys. C 4, 2064 (1971).

[16] S. L. Cunningham, Phys. Rev. B 10, 4988 (1974).

[17] W. Eberhardt, I. T. McGovern, E. W. Plummer, and J. E. Fisher, Phys. Rev. Lett. 44, 200 (1980).

[18] F. Herman (private conversation).

[19] D. R. Hamann, Phys. Rev. Lett. 42, 662 (1979).